Numerical investigations on unstable direct contact condensation of cryogenic fluids

K N Jayachandran[1,3], Arnab Roy[2] and Parthasarathi Ghosh[1]

[1] Cryogenic Engineering Centre, Indian Institute of Technology, Kharagpur, West Bengal-721302, India
[2] Department of Aerospace Engineering, Indian Institute of Technology, Kharagpur, West Bengal-721302, India

[3] E-mail: knjayachandran93@gmail.com

Abstract. A typical problem of Direct Contact Condensation (DCC) occurs at the liquid oxygen (LOX) booster turbopump exit of oxidiser rich staged combustion cycle based semi-cryogenic rocket engines, where the hot gas mixture (predominantly oxygen and small amounts of combustion products) that runs the turbine mixes with LOX from the pump exit. This complex multiphase phenomena leads to the formation of solid CO_2 & H_2O, which is undesirable for the functioning of the main LOX turbopump. As a starting point for solving this complex problem, in this study, the hot gas mixture is taken as pure oxygen and hence, DCC of pure oxygen vapour jets in subcooled liquid oxygen is simulated using the commercial CFD package ANSYS CFX®. A two fluid model along with the thermal phase change model is employed for capturing the heat and mass transfer effects. The study mainly focuses on the subsonic DCC bubbling regime, which is reported as unstable with bubble formation, elongation, necking and collapsing effects. The heat transfer coefficients over a period of time have been computed and the various stages of bubbling have been analysed with the help of vapour volume fraction and pressure profiles. The results obtained for DCC of oxygen vapour-liquid mixtures is in qualitative agreement with the experimental results on DCC of steam-water mixtures.

1. Introduction

To obtain high engine specific impulse, staged combustion cycle based rocket engines were developed where the outlet gas from the turbine of turbopump assembly undergoes combustion in the main combustion chamber instead of being vented out as in the gas generator cycle [1]. In a typical semi-cryogenic rocket engine working on staged combustion cycle, the booster turbine is run by the oxidiser rich combustion products from the pre-burner, which then mixes with LOX at the booster pump outlet [2]. This leads to a complex direct contact condensation problem with heat transfer and phase change, including solidification of the combustion products CO_2 & H_2O. The size of the solid contaminants entering the main turbopump should be small enough, so that it does not affect the structural integrity of the main pump blades. In contrast, the entire gas should be converted to liquid as the main pump is designed for handling incompressible fluids. So, the design of this direct contact condenser is an optimisation problem where the heat and mass transfer characteristics should not be so intense that the size of solid contaminants are outside the safety operational limits and at the same time, it should be

high enough to convert the entire gas into liquid. The goal of this paper is to obtain the overall heat and mass transfer characteristics when pure oxygen vapour jets/plumes condense in a pool of subcooled liquid oxygen, which provides an initial understanding to solve the original complex heat and mass transfer direct contact condensation problem.

2. Literature Review

DCC has been the focus of many researchers due to its application in Emergency Core Cooling (ECC's) systems of nuclear reactors, underwater propulsion systems, cooling towers, contact feed water heaters etc. [3]. The advantage of direct contact heat transfer equipment is its high efficiency and lower cost [4]. In the open literature, there are no works reported on DCC of oxygen gas jets in liquid oxygen and hence, literature review focuses mainly on the DCC of steam jets in subcooled water. The DCC of steam jets in subcooled water can be categorised as chugging, bubbling and jetting regimes based on steam mass flux [5]. Chan *et al.* [6] studied the unstable steam chugging regimes which occurs at very low mass fluxes, where water enters the steam pipe. This will give rise to pressure oscillations of very high amplitude that can create problems to the structure of the containing vessel. However, Simpson *et al.* [7] studied unstable DCC of steam jets at relatively higher subsonic speeds giving rise to bubble oscillation regimes consisting of the bubble formation, elongation, necking and collapsing stages. The necking effects give rise to pressure spikes of amplitude comparatively smaller than the steam chugging regimes [6]. Steam jetting regimes occur at choked nozzle conditions and gives rise to stable condensation regime [8]. In this paper, the focus is on DCC bubbling regimes whereas the chugging and jetting regimes will be studied in the future.

Numerical studies emerged as a powerful tool for analysing DCC in the past decade. Some of the pioneering works were done by Gulawani *et al.,* [9] [10] and Dahikar *et al.,* [11] on DCC of sonic steam jets in subcooled water. A two-fluid multiphase formulation with thermal phase change model was opted for these studies and the simulations were carried out on the commercial CFD package ANSYS CFX®. They obtained fairly good agreement between the experimental and numerical investigations. Shah *et al.,* [12] studied the DCC of supersonic steam jets in subcooled water using the commercial CFD package ANSYS Fluent®. In conjunction with the previous works, they have also used a two-fluid formulation with thermal phase change model for capturing the condensation effects. Thiele [13] used an open source CFD software OpenFOAM® to study the DCC phenomena using a VOF based multiphase formulation to capture the flow physics, but the code has not been validated with experimental data.

Based on the literature review, a two-fluid multiphase modelling approach with thermal phase change model was chosen for the present analysis. The details of the governing equations for the two-fluid model is available in section 3.2.

3. Numerical model

3.1. Geometry and boundary conditions

The geometry for the present study is taken from the case of Simpson *et al.* [7], where experimental studies on unstable DCC of steam jets in subcooled water has been performed. The selection of the geometry will help in future comparative studies and also for developing an experimental set-up for the oxygen vapour-liquid DCC studies. The dimensions of the given geometry are as shown in figure 1, where the vapour enters the tank through a cylindrical nozzle. It has been reported that the tank wall effects on the jet behaviour are negligible [7]. Hence, the tank dimensions are reduced and opening boundary condition is imposed on the reduced tank walls to take care of surrounding liquid effects. The mass flux at the boundary condition is computed to ensure a DCC bubbling regime. Oxygen vapour at saturated condition enters through the nozzle and the initial conditions inside the tank is kept as subcooled liquid oxygen at atmospheric pressure. The details of the boundary conditions are as shown in table 1.

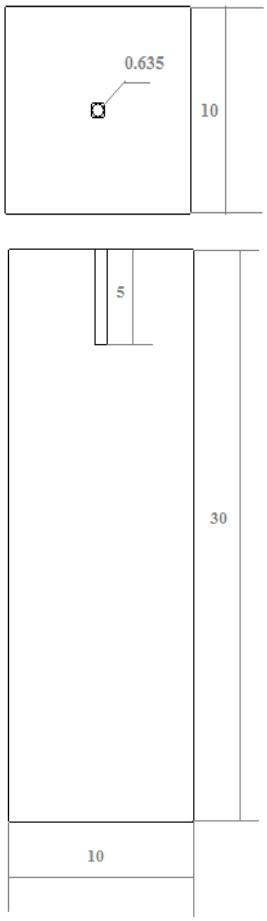

All dimensions are in cm

Figure 1. Geometry with dimensions.

Table 1. Boundary conditions.

	Value
Nozzle inlet mass flow rate (kg/s)	0.0051
Nozzle inlet temperature (K)	90.15
Liquid temperature (K)	65.15
Tank pressure (MPa)	0.1

3.2. Governing equations

A two-fluid multiphase formulation discretised using a finite-volume method has been chosen for the present analysis. A particle based multiphase model has been adopted for carrying out the simulations, where the interfacial area is calculated as,

$$A_{12} = \frac{6\alpha_2}{d_2} \tag{1}$$

The mean bubble diameter d_2 is obtained from the correlation by Anglart *et al.* [14], which is one of the most accepted correlations for subcooled boiling heat transfer applications. Moreover, this correlation proves to be a very good approximation for DCC cases as reported by Shah *et al.* [12].
The volume averaged-governing equations for the prescribed model are as follows,

3.2.1. Mass conservation. The continuity equation for both phases can be written as,

$$\frac{\partial}{\partial t}(\alpha_k \rho_k) + \nabla.(\alpha_k \rho_k \boldsymbol{U_k}) = S_{k,c} + \sum_{k=1}^{2} \Gamma_{12} \tag{2}$$

The two terms on the LHS refer to the unsteady and convective effects respectively. The first term on the RHS denotes the mass source term in the continuity equation which, in the present case is zero. The second term on the RHS indicates the mass source term due to phase change, the value of which is to be found out from the phase change model described in section 3.2.6.

3.2.2. Momentum conservation. Separate momentum equations are solved for both the phases as,

$$\frac{\partial}{\partial t}(\alpha_k \rho_k \boldsymbol{U_k}) + \nabla.\left(\alpha_k(\rho_k \boldsymbol{U_k} \otimes \boldsymbol{U_k})\right) = -\alpha_k \nabla p_k + \nabla.\left(\alpha_k \mu_k(\nabla \boldsymbol{U_k} + (\nabla \boldsymbol{U_k})^T)\right) + \sum_{k=1}^{2}(\Gamma_{12}^{+}\boldsymbol{U_2} - \Gamma_{21}^{+}\boldsymbol{U_1}) + S_{k,m} + M_{12}^{D} \quad (3)$$

The two terms on the LHS denote the unsteady and convective effects respectively. The first two terms on the RHS indicate the pressure gradient and shear stress effects respectively. The third term on the RHS refers to the momentum changes due to phase change. $S_{k,m}$ refers to the momentum source term which is zero for the case under study. The last term on the RHS takes account of the drag effects which is predicted by one of the most general and validated models by Schiller and Naumann [15] given as,

$$C_D = \frac{24}{Re}(1 + 0.15Re^{0.687}) \quad (4)$$

The term C_D refers to the drag coefficient and Re is the particle Reynolds number.

3.2.3. Energy conservation. Conservation equation for energy written in terms of the total enthalpy for both phases is given as,

$$\frac{\partial}{\partial t}\left(\alpha_k \rho_k h_{k,tot}\right) - \alpha_k \frac{\partial p}{\partial t} + \nabla.(\alpha_k \rho_k \boldsymbol{U_k} h_{k,tot}) = \nabla.(\alpha_k \lambda_k \nabla T_k) + \alpha_k \nabla.(\boldsymbol{U_k}.\tau_k) + S_{k,e} + Q_k + \sum_{k=1}^{2}\left(\Gamma_{12}^{+} h_{2s,tot} - \Gamma_{21}^{+} h_{1s,tot}\right) \quad (5)$$

The terms on LHS denote the unsteady and convective effects. The first term on the RHS denotes the conduction heat transfer term where λ_k is the thermal conductivity of the k^{th} phase. The second term on the RHS denotes the energy changes due to shear stress. $S_{k,e}$ denotes the energy source term which is again zero, as in the case of mass and momentum conservation. Q_k represents the interphase heat transfer from the other phase to the k^{th} phase. The last term on the RHS denotes the energy changes due to phase change which is calculated as discussed in section 3.2.6.

3.2.4. Volume constraint. The total volume fraction of the two phases should account to unity and the constraint is given as,

$$\sum_{k=1}^{2} \alpha_k = 1 \quad (6)$$

3.2.5. Pressure constraint. Both the phases are assumed to share the same pressure field by assuming instantaneous microscopic pressure equilibrium [16] as,

$$p_k = p \text{ for k = 1, 2} \quad (7)$$

Shared pressure assumption is a commonly adopted assumption in reported works [9] [10] [11] [12] on DCC of steam-water mixtures.

3.2.6. Thermal phase change model. To model phase change, a heat transfer model along with a simple heat balance based on saturation temperature has been adopted, which is known as the "Thermal phase change" model. A two resistance model has been adopted for the present case, where the heat transfer on both phases are modelled as,

$$q_1 = h_1(T_s - T_1) \quad (8)$$

$$q_2 = h_2(T_s - T_2) \quad (9)$$

The terms h_1 and h_2 are the heat transfer coefficients on the liquid and vapour side respectively. A zero equation model is used to model the heat transfer effects on the vapour side so that the vapour is

brought to saturation conditions at the interface. The heat transfer on the liquid side is modelled using the commonly adopted Ranz-Marshall model [17] as,

$$Nu = 2 + 0.6Re^{0.6}Pr^{0.3} \tag{10}$$

Using a simple heat balance to estimate the amount of mass transfer due to phase change as,

$$\dot{m}_{21} = \frac{(q_1+q_2)}{(h_{2s}-h_{1s})} \tag{11}$$

3.2.7. Turbulence model. A standard k-ε turbulence model has been used to model turbulence characteristics in the liquid phase. The transport equations for turbulent kinetic energy 'k' and turbulent dissipation rate 'ε' are given as,

$$\frac{\partial}{\partial t}(\alpha_k\rho_k k_k) + \nabla.\left[\alpha_k\left(\rho_k U_k k_k - \left(\mu + \frac{\mu_{tk}}{\sigma_k}\right)\nabla k_k\right)\right] = \alpha_k(P_k - \rho_k\varepsilon_k) + \Gamma_{12}(k) \tag{12}$$

$$\frac{\partial}{\partial t}(\alpha_k\rho_k\varepsilon_k) + \nabla.\left[\alpha_k\left(\rho_k U_k \varepsilon_k - \left(\mu + \frac{\mu_{tk}}{\sigma_\varepsilon}\right)\nabla\varepsilon_k\right)\right] = \alpha_k\frac{\varepsilon_k}{k_k}(C_{\varepsilon1}P_k - C_{\varepsilon2}\rho_k\varepsilon_k) + \Gamma_{12}(\varepsilon) \tag{13}$$

Γ_{12} (k) & Γ_{12} (ε) are the interphase transfer terms for k and ε respectively. The turbulent viscosity for the liquid phase 'μ_{t1}' is calculated as,

$$\mu_{t1} = c_\mu\rho_1\left(\frac{k_1^2}{\varepsilon_1}\right) \tag{14}$$

C_μ, $C_{\varepsilon1}$, $C_{\varepsilon2}$, σ_k, σ_ε are the various constants in turbulence modelling. Turbulence on the vapour side is modelled using the dispersed phase zero equation model [18] as,

$$\mu_{t2} = \frac{\rho_2}{\rho_1}\frac{\mu_{t1}}{\sigma} \tag{15}$$

3.3. Solution methodology

A coupled solver is used where an element based finite volume discretisation method has been adopted. The advection and turbulence terms were solved by a first order upwind scheme whereas the unsteady terms are solved using a first order backward Euler scheme. The selection of first order schemes for the present analysis is to avoid the stability issues associated with higher order schemes. Initially, steady simulations are performed until the residuals attain a steady state and the results thus generated are given as the initial condition for unsteady simulations. A time step size of 10^{-4} s has been chosen since the necking and collapsing phenomena occurs within fractions of a millisecond [7].

4. Results and Discussion

4.1. Grid independence study

To avoid errors due to coarse mesh sizes, a grid independence study was carried out. A blocked structured approach has been used to generate the grid using ICEM CFD®. Heat transfer coefficients at every time step are calculated and the averaged value over the entire time period is taken for the purpose of comparison. The various grids used for the test and the results of the grid independence study are as shown in table 2. The values of heat transfer coefficients at different grid sizes are also plotted as shown in figure 2. From the study, it can be inferred that case 3 and case 4 gives close enough results. So, to save computational time, case 3 has been taken as the optimum grid for further simulations.

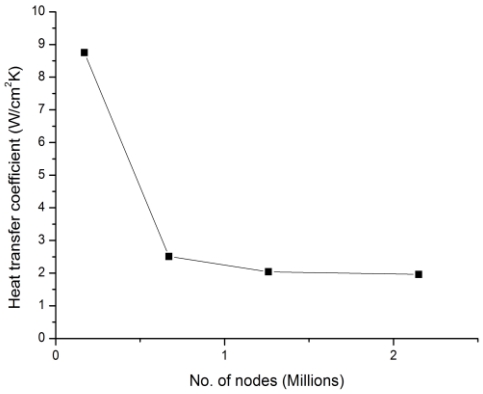

Figure 2. Grid independence study.

Table 2. Grid independence test.

Cases	Total number of nodes	Heat transfer coefficient (W/cm^2K)	Absolute percentage deviation (%)
Case 1	1, 70, 828	8.75	-
Case 2	6, 74, 574	2.51	71.31
Case 3	12, 57, 324	2.04	18.73
Case 4	21, 54, 903	1.96	3.92

4.2. Bubbling stages and heat transfer characteristics

The heat transfer characteristics of unstable DCC phenomena vary rapidly with the bubbling stages as shown in figure 3. The values of heat transfer coefficient are plotted for time period between 20 ms to 100 ms. While plotting the results, 0-20 ms is considered as the initial transients in the process of steady to unsteady transition and hence, the results after 20 ms is of importance to the designer.

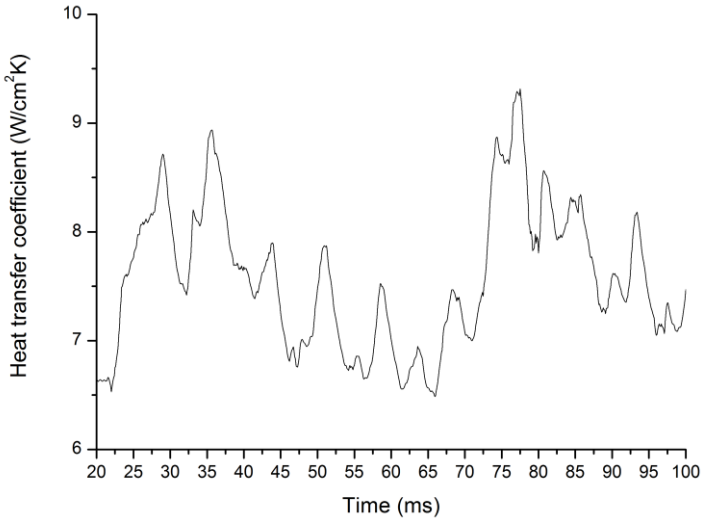

Figure 3. Variation of heat transfer coefficient with time.

It can be observed that the heat transfer coefficients are in the range of 6.5-9.5 W/cm^2K, which are much higher compared to the typical film condensation heat transfer coefficients of oxygen, which are in the range of 0.3-0.8 W/cm^2K [19]. A typical cycle of bubbling regime for a time period of 30 ms – 37 ms is taken for understanding the detailed flow physics and heat transfer characteristics.

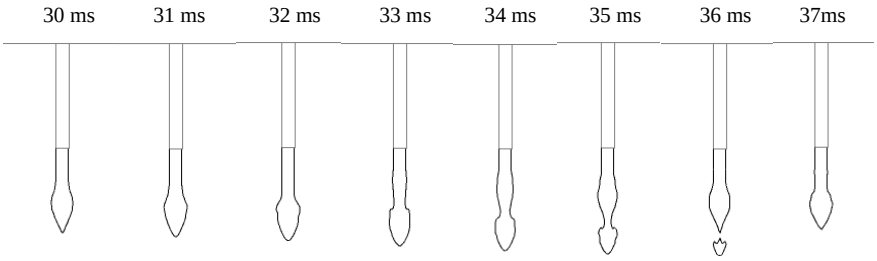

Figure 4. CFD results of plume shapes for a typical cycle of 30 ms – 37 ms.

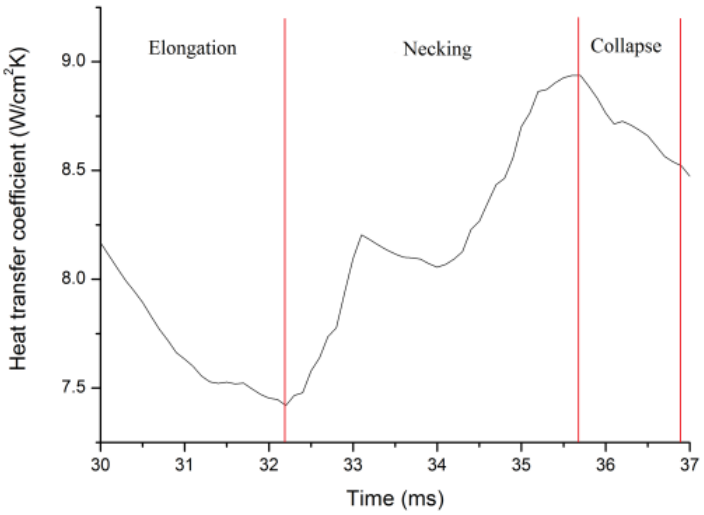

Figure 5. Heat transfer coefficients for a typical cycle of 30 ms – 37 ms.

It can be inferred from figure 4 and figure 5 that the heat transfer coefficient reaches a maximum during the necking stage and gradually decreases during the collapsing and elongation stages. It is due to the fact that the interfacial area decreases during the necking stage and hence, to maintain the same heat transfer rate, the heat transfer coefficient increases as given by the energy balance equation [7] [8]. Though interfacial area decreases during the collapsing stage, the bubble elongation stage initiates simultaneously supressing the effect of interfacial area reduction due to collapsing. Hence, there is a decrease in heat transfer coefficient during the collapsing and elongation stages. These results are in qualitative agreement with the experimental results for steam-water DCC obtained by Simpson *et al.*, [7]. The cycle repeats itself as the time advances, though the successive cycles may not be quantitatively similar. So, a statistical averaging over a large enough time history is required to obtain the heat transfer characteristics for the purpose of designing an oxygen vapour-liquid direct contact condenser.

4.3. Pressure oscillation studies

The values of pressure at an arbitrary point in the tank at a distance of 2.5 cm radial to the nozzle outlet is plotted as shown in figure 6.

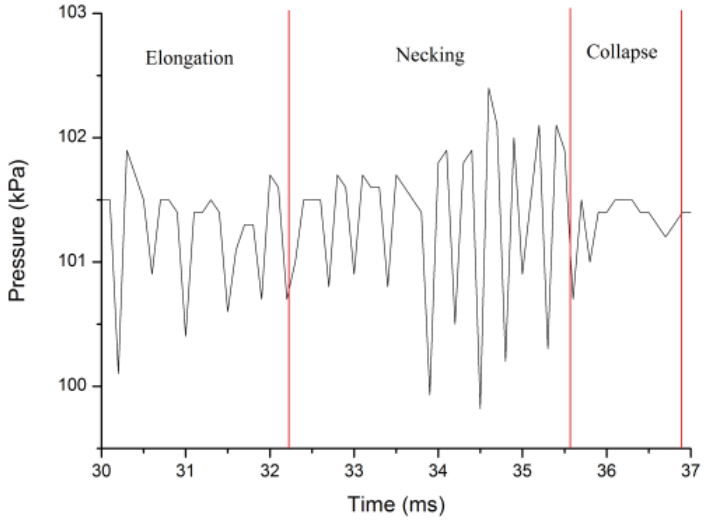

Figure 6. Pressure values for a typical cycle of 30 ms – 37 ms.

The pressure values show unstable oscillations and it can be observed that the peak to peak pressure amplitude is maximum during the necking stage. The interfacial area change is rapid during the necking stage which in turn gives rise to pressure oscillations of higher amplitudes. This is in agreement with the pressure spikes obtained for unstable DCC of steam-water mixtures [7]. The maximum peak to peak pressure amplitude observed is around 2-3 kPa which is much lower compared to the values of 20-40 kPa for steam chugging regimes [6]. So, it can be inferred that DCC bubbling regime may not provide a treat to the structural integrity of the condenser as compared to the DCC chugging regimes.

5. Conclusion

A two-fluid multiphase formulation with thermal phase change model has been employed to capture the DCC bubbling phenomena in oxygen vapour-liquid mixtures. It has been observed that DCC condensation provides a heat transfer coefficient of approximately 10 times higher than the typical film condensation heat transfer coefficient for oxygen. The various stages of bubbling such as elongation, necking and collapsing was observed with the help of vapour volume fraction profiles. It has been found that the heat transfer coefficient is maximum during the necking stage for oxygen vapour-liquid mixture which is also the case for reported works on steam-water mixtures. Pressure oscillations induced by bubbling was studied and it has been identified that peak to peak pressure oscillation amplitude is maximum at the necking stage. But, these peak to peak amplitudes are much lower compared to the DCC chugging regimes and hence can be considered comparatively safe from a structural design point of view. Further, a detailed quantitative assessment of heat transfer and pressure oscillation characteristics is necessary to develop a methodology for the design of oxygen vapour-liquid direct contact condenser.

Acknowledgment

The authors sincerely acknowledge the financial support provided by Liquid Propulsions Space Centre (LPSC), ISRO. The authors also acknowledge the computational support provided by Centre for Railway Research (CRR), IIT Kharagpur.

List of symbols

α – volume fraction
A – area, m^2
d – diameter, m
ρ – density, kg/m^3
U – velocity vector, m/s
S – source term
Γ – interphase transfer term, kg/m^3s
t – time, s
p – pressure, N/m^2
μ – viscosity, kg/ms
h – enthalpy, J/kg
λ – thermal conductivity, W/mK
τ – shear stress. N/m^2
k – turbulent kinetic energy, m^2/s^2
ε – turbulent energy dissipation rate, m^2/s^3
σ – turbulent Prandtl number

Subscripts
k – phase
1 – liquid phase
2 – vapour phase
tot – total
s – saturation
tk – turbulence term of k^{th} phase

Superscripts
+ - positive mass flow rate
D – drag force

References

[1] Demyanenko Y, Dmitrenko A, Ivanov A and Pershin V 2005 *41st AIAA/ASME/SAE/ASEE Joint Propulsion Conference & Exhibit* (Tucson, Arizona) **AIAA 2005-3946**.
[2] Pratt & Whitney 2001 *2nd Generation Reusable Launch Vehicle* Risk Reduction Requirements Program 2G RLV NRA 8-27: TA-3 & TA-4, Final Report, Revised.
[3] Sideman S and Moalem-Maron D 1982 *Advances in Heat Transfer* **15** 227-281.
[4] Kreith F and Boehm R F 1988 *Direct Contact Heat Transfer* (New York: Springer-Verlag Berlin Heidelberg) 2-3.
[5] Liang K S and Griffith P 1994 *Nuclear Engineering and Design* **147** 425-435.
[6] Chan C K and Lee C K B 1982 *International Journal of Multiphase Flow* **8(1)** 11-20.
[7] Simpson M E and Chan C K 1982 " *Journal of Heat Transfer* **104(2)** 271-278.
[8] Kim H Y, Bae Y Y, Song C H, Park J K and Choi S M 2001 International Journal of Energy Research **25** 239-252.
[9] Gulawani S S, Joshi J B, Shah M S, RamaPrasad C S and Shukla D S 2006 *Chemical Engineering Science* **61** 5204 – 5220.
[10] Gulawani S S, Dahikar S K, Mathpati C S, Joshi J B, Shah M S, RamaPrasad C S and Shukla D S 2009 *Chemical Engineering Science* **64** 1719 – 1738.
[11] Dahikar S K, Sathe M J and Joshi J B 2010 *Chemical Engineering Science* **65** 4606–4620.
[12] Shah A, Chughtai I R and Inayat M H 2010 *Fluid Flow and Transport Phenomena, Chinese Journal of Chemical Engineering* 18(4) 577-587.
[13] Thiele R 2010 *Modeling of Direct Contact Condensation with OpenFOAM* Royal Institute of Technology (Sweden).
[14] Anglart H, Nylund O, Kurul N and Podowski M Z 1997 *Nuclear Engineering and Design* **177** 215–228.
[15] Schiller L and Naumann, Z A 1933 *Z. Ver. Deutsch* **77** 318.
[16] Yeoh G H and Tu J 2010 *Computational Techniques for Multi-Phase Flows* (Oxford, UK: Butterworth-Heinemann) 49-50.
[17] Ranz W E and Marshall W R 1952 *Chem.Eng.Prog.* **48** 141–146; 173–180.
[18] Sato Y and Sekoguchi K 1975 *International Journal of Multiphase Flow* **2(1)** 79-95.
[19] Haselden G G and Prosad S 1949 *Trans. Inst. Chem. Eng. (London)* **27** 195.